SECURITY CLASSIFICATION OF THIS PAGE

(2)

NTATION PAGE

Form Approved
OMB No 0704 0188

AD-A237 507

1a REPORT SECURITY CLASSIFICATION: Unc

1b RESTRICTIVE MARKINGS

2a SECURITY CLASSIFICATION AUTHORITY

3 DISTRIBUTION/AVAILABILITY OF REPORT
Approved for public release and sale; its distribution is unlimited.

2b DECLASSIFICATION/DOWNGRADING SCHEDULE

4 PERFORMING ORGANIZATION REPORT NUMBER(S)
Technical Report No. 102

5 MONITORING ORGANIZATION REPORT NUMBER(S)

6a NAME OF PERFORMING ORGANIZATION
Purdue University
Department of Chemistry

6b OFFICE SYMBOL (If applicable)

7a NAME OF MONITORING ORGANIZATION
Division of Sponsored Programs
Purdue Research Foundation

6c ADDRESS (City, State, and ZIP Code)
Purdue University
Department of Chemistry
West Lafayette, IN 47907

7b ADDRESS (City, State, and ZIP Code)
Purdue University
West Lafayette, IN 47907

8a NAME OF FUNDING/SPONSORING ORGANIZATION
Office of Naval Research

8b OFFICE SYMBOL (If applicable)

9 PROCUREMENT INSTRUMENT IDENTIFICATION NUMBER
Contract No. N00014-91-J-1409

8c ADDRESS (City, State, and ZIP Code)
800 N. Quincy Street
Arlington, VA 22217

10 SOURCE OF FUNDING NUMBERS

PROGRAM ELEMENT NO.	PROJECT NO.	TASK NO	WORK UNIT ACCESSION NO

11 TITLE (Include Security Classification)
Comparisons Between Scanning Tunneling Microscopy and Outer-Sphere Electron-Transfer Rates at Pt(111) Surfaces Coated with Ordered Iodine Adlayers

12 PERSONAL AUTHOR(S)
S.-C. Chang, S.-L. Yau, B.C. Schardt, and M.J. Weaver

13a TYPE OF REPORT	13b TIME COVERED	14 DATE OF REPORT (Year, Month, Day)	15 PAGE COUNT
Technical	FROM _____ TO _____	May 31, 1991	

16 SUPPLEMENTARY NOTATION

17 COSATI CODES			18 SUBJECT TERMS (Continue on reverse if necessary and identify by block number)
FIELD	GROUP	SUB-GROUP	correlations between the outer-sphere electron-transfer kinetics, real-space iodine adlattice structures, unmodified mercury and Pt(111) electrodes

19 ABSTRACT (Continue on reverse if necessary and identify by block number)

Rate parameters are reported for the electroreduction of eight $Co^{III}(NH_3)_5X$ complexes at ordered Pt(111) surfaces coated with iodine adlayers whose structures are characterized by scanning tunneling microscopy (STM) in order to explore possible correlations between the outer-sphere electron-transfer kinetics and the spatially resolved adlattice properties as revealed by STM. The sixth ligands: X = NH_3, F^-, OSO_3^{2-}, OH_2, acetate, and three cyclic organic carboxylates, were selected so to vary the reactant charge, and hence the magnitude of electrostatic double-layer effects, and to examine the effect of potential organic mediators. The ordered Pt(111) surfaces were prepared by flame annealing, followed by cooling in a stream of nitrogen over iodine crystals (cf ref. 5). Three types of iodine adlayer structures could be formed, one having a $(\sqrt{7} \times \sqrt{7})R19.1°$ unit cell and two coexisting structures with (3 x 3) symmetry, as identified by STM. The real-space iodine adlattice structures extracted from these data are discussed (cf ref. 4) along with spatially-dependent electron-tunneling parameters for each iodine adsorption site, also obtained from STM. For

20 DISTRIBUTION/AVAILABILITY OF ABSTRACT
☐ UNCLASSIFIED/UNLIMITED ☐ SAME AS RPT. ☐ DTIC USERS

21 ABSTRACT SECURITY CLASSIFICATION

22a NAME OF RESPONSIBLE INDIVIDUAL

22b TELEPHONE (Include Area Code)

22c OFFICE SYMBOL

DD Form 1473, JUN 86 Previous editions are obsolete. SECURITY CLASSIFICATION OF THIS PAGE

19. (cont.)

reactants containing only inorganic ligands, the observed (apparent) rate constants k_{app} are markedly (3–5 fold) larger on the ($\sqrt{7}$ x $\sqrt{7}$) adlayer. This more facile electron mediation provided by the ($\sqrt{7}$ x $\sqrt{7}$) versus the (3 x 3) adlayers is rationalized in terms of the preponderance of threefold hollow iodine atoms in the former structure. Somewhat more facile electroreduction on the iodine adlayer surfaces are observed for complexes containing aromatic carboxylate substituents, although the kinetics in these cases are insensitive to the adlayer structure. This is attributed to the presence of specific interactions between the aromatic rings and the iodine adlayer. Comparisons are also made with corresponding rate parameters obtained at unmodified mercury and Pt(111) electrodes.

OFFICE OF NAVAL RESEARCH

Contract No. N00014-91-J-1409

Technical Report No. 102

Comparisons Between Scanning Tunneling Microscopy and Outer-Sphere Electron-Transfer Rates at Pt(111) Surfaces Coated with Ordered Iodine Adlayers

by

S.-C. Chang, S.-L. Yau, B.C. Schardt and M.J. Weaver

Prepared for Publication

in the

Journal of Physical Chemistry

Purdue University

Department of Chemistry

West Lafayette, Indiana 47907

May 1991

Comparisons Between Scanning Tunneling Microscopy and Outer-Sphere Electron-Transfer Rates at Pt(111) Surfaces Coated with Ordered Iodine Adlayers

Si-Chung Chang, Shueh-Lin Yau, Bruce C. Schardt*

and Michael J. Weaver*

Dept. of Chemistry, Purdue University

West Lafayette, IN 47907

J. Phys. Chem.

submitted July 2, 1990

revised November 19, 1990

ABSTRACT

Rate parameters are reported for the electroreduction of eight $Co^{III}(NH_3)_5X$ complexes at ordered Pt(111) surfaces coated with iodine adlayers whose structures are characterized by scanning tunneling microscopy (STM) in order to explore possible correlations between the outer-sphere electron-transfer kinetics and the spatially resolved adlattice properties as revealed by STM. The sixth ligands: X = NH_3, F^-, OSO_3^{2-}, OH_2, acetate, and three cyclic organic carboxylates, were selected so to vary the reactant charge, and hence the magnitude of electrostatic double-layer effects, and to examine the effect of potential organic mediators. The ordered Pt(111) surfaces were prepared by flame annealing, followed by cooling in a stream of nitrogen over iodine crystals (cf ref. 5). Three types of iodine adlayer structures could be formed, one having a $(\sqrt{7} \times \sqrt{7})R19.1^\circ$ unit cell and two coexisting structures with (3 x 3) symmetry, as identified by STM. The real-space iodine adlattice structures extracted from these data are discussed (cf ref. 4) along with spatially-dependent electron-tunneling parameters for each iodine adsorption site, also obtained from STM. For reactants containing only inorganic ligands, the observed (apparent) rate constants k_{app} are markedly (3-5 fold) larger on the $(\sqrt{7} \times \sqrt{7})$ adlayer. This more facile electron mediation provided by the $(\sqrt{7} \times \sqrt{7})$ versus the (3 x 3) adlayers is rationalized in terms of the preponderance of threefold hollow iodine atoms in the former structure. Somewhat more facile electroreduction on the iodine adlayer surfaces are observed for complexes containing aromatic carboxylate substituents, although the kinetics in these cases are insensitive to the adlayer structure. This is attributed to the presence of specific interactions between the aromatic rings and the iodine adlayer. Comparisons are also made with corresponding rate parameters obtained at unmodified mercury and Pt(111) electrodes.

An intriguing issue in surface electrochemistry concerns the relationships between the efficiency of electron transfer to and from solution redox couples at metal surfaces and the electronic and molecular structure of the interfacial region. The significance of this question stems in part from the expectation that some electrochemical processes may proceed via nonadiabatic pathways, i.e. where the electron-tunneling probability within the transition state, κ_{el}, is less than unity, thereby impeding the reaction rate.[1] In addition, rate-surface environment variations can often arise from differences in the reaction energetics, associated especially with solvent reorganization and interfacial work terms ("double-layer" effects). Such electrochemical reactivity-interfacial structural correlations are profitably pursued at ordered monocrystalline metal surfaces in view of their structural definition and uniformity. Such electrochemical kinetic measurements, however, are rare.

An interesting opportunity to examine such issues is provided by ordered Pt(111) surfaces covered by iodine adlayers. The electrochemical properties of iodine-coated platinum are well known[2]; iodide (or iodine) yields densely packed adlayers held tenaciously via relatively strong covalent bonds to the metal substrate. Such adlayers oblige electrochemical reactions following facile inner-sphere pathways to proceed instead via much slower outer-sphere routes by eliminating coordinative access to the metal surface.[3] Recently, two of us have obtained detailed atomic-resolution images of iodine adlayers on Pt(111) in air[4a] and in an aqueous electrochemical environment[4b] by means of scanning tunneling microscopy (STM). The ordered Pt(111)/I surfaces are prepared by annealing the platinum crystal in a oxy-hydrogen flame followed immediately by cooling in a stream of nitrogen over iodine crystals.[5] The distinct iodine adlattices thus formed can be characterized clearly by subsequent STM imaging in air or in aqueous solution.[4] If the Pt(111) surface

is held >3 cm above the iodine during cooling, an adlattice having a ($\sqrt{7}$ x $\sqrt{7}$)R19.1° unit cell [abbreviated here to ($\sqrt{7}$ x $\sqrt{7}$)] is observed, with a fractional iodine coverage θ_I = 0.43. When this distance is ca 1 cm or less (depending on the N_2 flow rate), a mixture of two other adlattice structures both having a (3 x 3) unit cell, with a slightly higher iodine coverage (θ_I = 0.44), are obtained instead.[4a] The structures of these three adlattices are markedly different.[4a] Of the three iodines in the ($\sqrt{7}$ x $\sqrt{7}$) unit cell, two occupy threefold hollow sites, and one iodine is atop a single Pt atom. The (3 x 3) adlattice that was characterized initially,[4a] termed here (3 x 3)-hex (hex = hexagonal), contains three iodines in twofold bridging sites and one atop iodine. The alternative (3 x 3) adlattice, which is present simultaneously to a roughly equal extent with (3 x 3)-hex, features only one threefold hollow iodine in the unit cell, with the remaining three iodines occupying shifted ("asymmetric") atop sites. The assignment of this structure, denoted here (3 x 3)-asym, is described for the first time below.

Since these adlayer structures are inferred from atomic-level spatial variations in the electron-tunneling current to the STM tip, one can anticipate that such differences might also be manifested in variations in the electron-tunneling rates to nearby solution redox species. While only spatially averaged electron-transfer rates can be obtained by conventional electrochemical means, significant differences in the overall electron-mediating properties of the three adlayer structures might thereby be anticipated.

We report here atomic-level electron-tunneling properties derived from STM for individual iodine adsorbate sites in the three adlattice structures formed on ordered Pt(111). Also provided are electrochemical kinetic data for the reduction of a number of cobalt(III) pentaammine complexes $Co^{III}(NH_3)_5X$ on these iodine-modified Pt(111) surfaces, with the objective

of exploring such possible rate-surface structural correlations. Cobalt(III) ammine electroreductions provide insightful probe reactions for this purpose for several reasons. The irreversible nature of the Co(III) to Co(II) conversion eases considerably the task of obtaining reliable rate-potential data, and the charge type and overall reactant structure can both be altered substantially by varying the sixth ligand X, enabling the role of interfacial environmental effects[3,6-9] to be evaluated. In particular, the reactant trio $Co(NH_3)_6^{3+}$, $Co(NH_3)_5F^{2+}$ and $Co(NH_2)_5OSO_3^+$ are employed here, as before,[3b,6a,7,9] so to afford a distinction between electrostatic and other environmental ("double-layer") effects upon the measured kinetics. Several $Co^{III}(NH_3)_5X$ complexes with organic carboxylate ligands X are also examined here so to explore possible specific interaction effects between such groups and the iodine-coated surfaces (cf ref. 8).

Experimental Section

The Pt(111) surface used for most of the present experiments was a ca 1 cm diameter disk, oriented within 0.5° (Johnson-Matthey Co.) Electrical connection was via a Pt wire spot-welded to the rear of the polished crystal face. As noted above, the crystal surface was ordered by annealing for ca 1 min in a oxy-hydrogen flame. This was followed immediately by cooling within an enclosed vessel in an upward N_2 stream above iodine crystals so to yield either ($\sqrt{7}$ x $\sqrt{7}$) or (3 x 3) adlayers, as verified by STM (vide infra). The crystal was then mounted on a glass holder by means of Teflon tape, so to leave only the crystal face exposed (cf ref. 10). For kinetic measurements on bare rather than iodine-coated Pt(111), the crystal was immersed in 0.1 M $HClO_4$ at -0.25 V and the iodine adlayer displaced by bubbling in CO. The solution was then flushed thoroughly with fresh 0.1 M $HClO_4$ so to remove solution CO and iodine, and the CO adlayer removed electrooxidatively at 0.5 V vs. SCE. The well-ordered nature of the Pt(111) surface

was confirmed from the well-known "butterfly" voltammetric features (see refs. 5 and 10 for details).

The electrochemical kinetics were evaluated by means of linear sweep voltammetry with the Pt(111) crystal suspended within a conventional electrochemical cell with a Pt wire counter electrode, largely as described in ref. 9 (see below for details). The reference electrode, separated from the main compartment by a glass frit, was a saturated calomel electrode containing NaCl rather than KCl, but all potentials are quoted here versus the conventional SCE. A EG and G Model 273 potentiostat was used for the voltammetric measurements. As before, acidified aqueous 0.1 M $NaClO_4$ was chosen as the supporting electrolyte in view of the weak specific adsorption of perchlorate and for consistency with earlier measurements.[7-9] (The ca 5 mM $HClO_4$ that was present buffered the solution acidic so to prevent the precipitation of Co(II) product hydroxy species on the electrode surface.[6a,7]) The solution was thoroughly purged and then blanketed with nitrogen prior to the electrochemical measurements. The sodium perchlorate (G. F. Smith) was recrystallized from water. The Co(III) complexes were synthesized as crystalline perchlorate salts as outlined in refs. 6a and 8. The Co(III) concentrations were around 1 mM. Water was purified by means of a Milli Q system (Millipore Inc.). All kinetic measurements reported here were made at 23±1°C.

The STM images for the Pt(111)/iodine adlayers in air were acquired by using a Nanoscope II instrument (Digital Instruments, Santa Barbara, CA). The microscope preamplifier was replaced with one of feedback design to circumvent distortions in the measured current by the 1 mV/nA voltage burden of the original shunt current preamplifier.[11] Unless stated otherwise, STM experimental images were obtained by using the "constant height" mode.

A 2 nm terrace machined across the back face of the Pt crystal along with a mating grove machined into the sample mount of the STM provided a

simple and reliable method of fixing the azimuthal orientation of the Pt crystal during imaging. Laue back reflection X-ray photographs were then used to determine the azimuthal orientation of the Pt crystal as mounted on the STM stage. The (111) type crystallographic directions were determined to be 49°, 169°, and 289° from the x-axis scan direction of the microscope (horizontal in the images shown here). This orientation is such that the rows of platinum atoms can be expected at 19°, 79°, and 139°.

RESULTS AND DISCUSSION

Electron-Tunneling Properties of Iodine Adlattices from STM

As already noted, either ($\sqrt{7}$ x $\sqrt{7}$) or (3 x 3) iodine adlayers can be formed reproducibly on ordered Pt(111) by controlling the iodine dosage appropriately following the flame-annealing step. In the following, the initial report on this system[4a] is expanded by providing an unambiguous correlation between the spots in the STM images with specific iodine adsorption sites. We will also provide an accounting of the topographic and electronic contributions to the variation of the tunneling currents across the surface (x,y directions).

Figure 1 shows a typical atomic resolution STM image of the ($\sqrt{7}$ x $\sqrt{7}$) adlattice. (See the caption for experimental conditions). The presence of a ($\sqrt{7}$ x $\sqrt{7}$)R 19.1° unit cell, originally deduced by low-energy electron diffraction (LEED),[12] is easily verified by STM.[4a] Further, the STM images clearly indicate the presence of iodine atoms in three different adsorption sites, corresponding to the three types of spots with differing intensities seen in Fig. 1.[4a] The "brightest" spots (i.e. where the tunneling current is highest) arise from iodine present at atop sites (i.e. bound to a single surface Pt atom) as indicated. The two additional spots in each unit cell both refer to iodine bound to threefold hollow sites,[4a] corresponding to hexagonal close packed (hcp) and face-centered cubic (fcc) coordination.[4a]

The hcp and fcc sites are characterized by the presence of a second-layer Pt atom and an octahedral hole, respectively, immediately underneath the iodine. A clear identification of the brighter and weaker spots with iodine bound to the hcp and fcc sites, respectively, was achieved by obtaining STM images where the azimuthal orientation at the underlying Pt substrate was known, as described above. (This assignment is the opposite of the original deduction,[4a] made without benefit of such additional information). The derived real-space structure is shown schematically in Fig. 2A.

Of particular interest in the present work are the variations of the STM tunneling currents across the surface (x,y directions), especially between specific iodine adsorption sites, and as a function of the surface-tip separation, d (z direction). Such information can be extracted from z - x cross-sections through STM images observed for different constant heights (d values) as obtained by employing various set-point currents, i_o, and bias voltages, V_b. At least when using etched tungsten or Pt/Ir tunneling tips, images of the ($\sqrt{7}$ x $\sqrt{7}$) adlattice similar to Fig. 1 were obtained for i_o values above 5 nA and V_b values below 20 mV. Figure 3 illustrates such z - x data obtained for the ($\sqrt{7}$ x $\sqrt{7}$) iodine adlattice for four "gap resistance" values R_g (= V_b/i_o) as indicated, with the x axis taken in the direction of the long diagonal of the unit cell. (As seen in Figs. 1 and 2A, this axis passes conveniently through the centers of all three types of iodine adsorption sites: atop, hcp and fcc threefold hollow sites). The z-axis scale in Fig. 3 was deduced from the observed variations in tunneling current, i_c, relative to the set-point current by using the well-known formula[13]

$$i_c = i_o \exp [- \beta(d - d_o)] \qquad (2)$$

Here d and d_o are the surface-tip separations corresponding to i_c and i_o, and β is the usual "inverse tunneling decay length", familiar from both the STM and molecular electron-transfer literature.[13,14] An average value of β

of 9±1 nm^{-1} (= 0.9$Å^{-1}$) for the ($\sqrt{7}$ x $\sqrt{7}$) adlattice was obtained by fitting to Eq.(2) the d-dependent currents acquired by ramping the tip-surface separation distance from d_o to (d_o + 2.0 nm). While this value of β is somewhat smaller than those typical of STM experiments at metal-vacuum surfaces,[14a] it is comparable to the values commonly observed for molecular electron tunneling.[14b-d] While three of the z-x plots in Fig. 3 were extracted from the usual "constant-height" mode images by using this procedure, the trace shown for R_g = 100 KΩ was obtained instead from STM data acquired in the "constant current" mode. The latter yields z-x displacements directly. The closely comparable z-x corrugations that are seen to be obtained by using these two approaches (Fig. 3) confirms the validity of the above procedure.

Inspection of Fig. 3 shows that the maximum tunneling currents at a given d value are obtained for the atop iodines, as expected from the STM image in Fig. 1. The hcp iodines also yield a clearcut z-x maximum, having a z-displacement from 0.04 to 0.09 nm below that for the atop site. Given that the STM images refer to a "constant height" of the tip above the substrate surface, this difference in imaging intensity between the hcp and atop sites can be understood partly from the 0.055 nm corrugation between these iodines anticipated from surface atomic models. (This estimate assumes that the iodine atomic radius is the same in both adsorption sites, and that the Pt surface lattice does not undergo relaxation upon iodine adsorption). In other words, the tunneling currents at the hcp and atop sites are not greatly different once the tip-surface distance is corrected for the anticipated z-displacement between these iodines, Interestingly, however, the difference in the z-x maxima between these sites tends to increase for larger R_g values, i.e., as the tip-surface separation d is increased (Fig. 3). This indicates that the tunneling current to the hcp site diminishes more sharply with increasing d than for the atop site (i.e., β is larger for the

former site).

In contrast to the hcp and fcc sites, electron tunneling at the fcc site is sufficiently weak so that a z-x maximum is barely observed, especially for larger R_s values (Fig. 3). Since the fcc and hcp iodines should be situated at virtually identical positions in the z plane, this finding indicates that the electron-tunneling efficiency at fcc iodines is intrinsically lower than for hcp as well as atop sites in the ($\sqrt{7}$ x $\sqrt{7}$) adlattice structure.

Figures 4 and 5 show typical STM images of the (3 x 3)-hex and (3 x 3)-asym adlattices. These two adlattices were generally found to coexist to a comparable extent on the Pt(111) surface; no preparative recipe was found to yield exclusively one or the other structure. Similar results were obtained for (3 x 3) adlayers in an in-situ electrochemical environment (cf ref. 4b). Even though the iodine coverage is only slightly higher in the (3 x 3) versus the ($\sqrt{7}$ x $\sqrt{7}$) adlayers, 0.44 versus 0.43, the structures are markedly different.

The deduction of the (3 x 3)-hex structure from the STM images has been discussed previously.[4a] As shown in Fig. 2B, the unit cell consists of a single atop iodine together with three iodines in equivalent twofold bridge sites. Similarly to the ($\sqrt{7}$ x $\sqrt{7}$) adlayer, the atop iodine yields the most intense STM image; as before, this can be attributed in part to the significantly (0.045 nm) higher z-position of the atop versus the twofold bridging iodines that is expected geometrically. This point is made more quantitatively in the typical z-x plots for (3 x 3)-hex shown in Fig. 6A, taken along an axis so to encompass equal numbers of atop and twofold bridging iodines (long axis of Fig. 4). As in Fig. 3, the z-axis is converted into a surface-tip distance scale by using Eq.(2) along with an estimate of β. The latter was determined to be 9 nm^{-1} for the (3 x 3)-hex adlattice [i.e. essentially identical to that for ($\sqrt{7}$ x $\sqrt{7}$)]. Inspection of Fig. 6A shows that the ef-

fective "height" of the twofold bridging iodine is about 0.08 nm lower than for the atop iodine. The "intrinsic" electron-tunneling efficiency at the bridge sites is therefore not greatly different from (although probably somewhat lower than) that at the atop site.

Details of the additional (3 x 3) adlayer structure, (3 x 3)-asym, have not been given previously. The STM images (e.g. Fig. 5) show the presence of three equivalent iodine atoms arranged in such a way so that six such atoms surround a central "hole". The positions of these iodines with respect to the underlying Pt substrate could be deduced accurately from a knowledge of the Pt lattice parameters combined with (3 x 3) STM images obtained over surface regions where (3 x 3)-hex and -asym domains are juxtaposed (as in Fig. 7A). Such a computer-based data analysis places the three equivalent iodines seen in the STM images in identical "asymmetric atop" sites, each displaced by 0.06 nm from a symmetric atop position. The "central hole" in the STM image is located precisely in a fcc threefold hollow site on the Pt(111) substrate. The presence of iodine in this site together with the asymmetric atop sites yields the correct total iodine coverage (0.44), and is also consistent with the weak images observed for iodine in the fcc threefold site within the ($\sqrt{7}$ x $\sqrt{7}$) adlattice. The (3 x 3)-asym structure is therefore deduced to be as shown in Fig. 2C: the unit cell contains four iodines, three in asymmetric atop sites and one in a fcc threefold hollow site.

A typical z-x plot for the (3 x 3)-asym adlattice, taken along an axis containing equal numbers of atop and threefold hollow sites, is shown in Fig. 6B. The β value used, as before, to transpose the observed current variations into the z-scale shown, was determined again to be 9 nm^{-1} for (3 x 3)-asym. As anticipated from the STM images (Fig. 5), Fig. 6B shows that only the asymmetric atop iodine yields a z-x maximum, the fcc

site being associated with a current *minimum*. This observation, however, is not surprising given the weak imaging behavior of the fcc site in the ($\sqrt{7}$ x $\sqrt{7}$) adlattice combined with the "spillover" from the intense imaging of the nearby trio of atop iodines.

For the present purposes, it is desirable to extract an estimate of the relative electron-tunneling efficiencies of the symmetrical and asymmetric atop iodines. In principle, this could be obtained by inspecting STM images of (3 x 3) adlayers that traverse domain boundaries, as in Fig. 7A. An example of such a z-x plot, extracted from the STM image in Fig. 7A along the direction shown by the arrow, is shown in Fig. 7B. While instructive, these data illustrate how the feedback-driven control of the surface-tip separation, d_o, can influence STM imaging. It is important to note that while ideally d_o is desired to be held constant, in practice only the set-point current is controlled (the absolute surface-tip separation is, of course, unknown). As the tip scans (from right to left in Fig. 7A) so to traverse the domain boundary between the hex and asym adlattices, higher tunneling currents are initially obtained, as seen from the peak amplitudes of the z-x plot (Fig. 7B) or from the greater intensities of the asymmetric atop iodine images close to the domain boundary (Fig. 7A). Further to the left of the domain boundary, into the (3 x 3)-asym domain, the asymmetric atop iodine images become less intense (Fig. 7A), and therefore the peak currents diminish. This results from the above feedback effect, the surface-tip separation being increased so to maintain the chosen set-point current. Consequently, we can roughly deduce that the electron-tunneling efficiencies are probably slightly higher on the asymmetric relative to the symmetric iodines. The vagaries of the STM feedback circuitry, however, vitiate quantitative comparison of tunneling currents across the extended x-direction tip displacements required for this purpose.

In summary, then, the predominant contributions to the STM imaging provided by the atop iodines relative to those at twofold bridging and hcp threefold sites can be attributed at least partly to the higher z-plane position of the former adsorbate atoms. Iodines in fcc threefold sites engender intrinsically weaker electron tunneling, and there is some evidence that asymmetric atop iodines have more efficient tunneling properties. In the context of the present work, however, it should be borne in mind that several other factors may well influence such apparent z-corrugations in STM images. The most well-known factor is compressive forces between the tip and the sample, which yield especially anomalous corrugations for graphite surfaces.[15] The form of the z-x plots can also be sensitive to the condition of the tunneling tip as well as to the imaging conditions. For example, we have observed distinctly different images for the present systems when cleaved, rather than etched, tungsten tips are employed. Consequently, then, the quantitative interpretation of such z-x traces purely in terms of electron-tunneling properties of the metal surface may well be questionable.

Electrochemical Kinetics

Pertinent electrochemical rate data gathered in the present study are summarized in Table I, in the form of apparent (i.e. double-layer uncorrected) rate constants, k_{app} (cm s^{-1}), together with corresponding transfer coefficients α_{app}. [The latter denote the k_{app} - electrode potential (E) dependence, so that $\alpha_{app} = -(RT/F)(d \ln k_{app}/dE)$]. These parameters were determined from the linear sweep voltammograms as follows.[9] Values of k_{app} were evaluated at the voltammetric peak potential for a given voltammetric sweep rate, ν(V s^{-1}), as well as at lower overpotentials corresponding to one half and one quarter of the peak current, $E_{p/2}$ and $E_{p/4}$, respectively, by using the relation[9]

$$\log k_{app} = K + \log(\alpha_{app}\ \nu DF/RT)^{\frac{1}{2}} \qquad (3)$$

Here D is the Co(III) diffusion coefficient, and the constant K equals 0.339, -0.469, or -0.851 at potentials equal to E_p, $E_{p/2}$, and $E_{p/4}$, respectively. The required values of α_{app} were obtained from the relative k_{app} values at E_p, $E_{p/2}$, and $E_{p/4}$. Variations in the voltammetric sweep rate from 0.05 to 0.5 V s^{-1} thereby yielded segments of log k_{app} -E (i.e., Tafel) plots that spanned about 0.2 V, from k_{app} values of ca 5 x 10^{-4} to 2 x 10^{-2} cm s^{-1}. The required diffusion coefficients were as obtained earlier;[6-8] (for the present reactants D ≈ 7(±2) x 10^{-6} cm^2 s^{-1}). The k_{app} values listed in Table I refer to the common electrode potential -0.1 V vs. SCE; this value was selected so to facilitate data intercomparison, while minimizing the extent of data extrapolation that was involved. The k_{app} values obtained at the iodine-coated Pt(111) surfaces were typically reproducible at least within ±30%. The kinetics were essentially unaffected by the addition of up to 20 mM solution iodide, confirming the tenacious irreversible binding of the iodine adlayers and the absence of significant contributions to the kinetics from "pinholes" in the adsorbate layer. Further, the STM adlayer images, both in air and in aqueous solution,[4] exhibit large well-ordered domains having uniform structures over dimensions limited only by the average substrate terrace widths, ca 30 nm. The STM images for the in-situ surface[4b] are also unaffected by the presence of solution iodide.

Rate data were obtained for eight Co(III) ammines, $Co^{III}(NH_3)_5X$. Four of these, X = NH_3, F^-, OSO_3^{2-}, and OH_2, have been employed extensively in previous studies[3b,6,7,9]; the examination of such reactants having roughly comparable reactivities yet differing net charges enables the importance of diffuse-layer effects to be gauged.[3b,6,7] The other four reactants each contain organic carboxylate ligands: CH_3COO^-, p-$C_5H_4NCOO^-$, and $C_5H_9CH_2COO^-$. The last three carboxylates, containing benzene, pyridine, and cyclopentane

groups, respectively, enable the kinetic effects of such "hydrophobic" reactant moieties to be assessed (cf ref. 8).

Rate parameters are listed in Table I for each reactant in acidified 0.1 M $NaClO_4$ on Pt(111) coated with iodine adlayers having both the ($\sqrt{7}$ x $\sqrt{7}$) and (3 x 3) structures, as confirmed by STM measurements in air both before and after the kinetic measurements. [These surface structures are abbreviated to Pt/I($\sqrt{7}$) and Pt/I(3 x 3) in Table I]. Comparison between the rate data for each reactant in these two iodine adlayers reveals that in most cases the I($\sqrt{7}$ x $\sqrt{7}$) adlayer yields markedly (3-5 fold) larger k_{app} values than are observed on the I(3 x 3) surface. The only exceptions are the reactants containing the aromatic carboxylate substituents, for which the rate constants for a given reaction are virtually the same on the two adlayer surfaces (Table I).

Corresponding rate data obtained after the addition of 50 mM $La(ClO_4)_3$ are also listed in Table I. Given that the iodine adlayer might be expected to carry a partial negative charge, the addition of La^{3+} should diminish substantially the negative diffuse-layer potential, and therefore the anticipated accelerating influence of the diffuse layer towards electroreduction of the cationic reactants (see, for example, ref. 17). Consistent with this explanation, significant (up to 10 fold) rate decelerations are observed in some cases upon La^{3+} addition (Table I). However, the magnitude of such apparent diffuse-layer effects is not entirely proportional to $(Z_r - \alpha)$, where Z_r is the net reactant charge. Such a correlation with $(Z_r - \alpha)$ would be expected, and is indeed observed, under more conventional conditions on mercury surfaces.[3a,6,7] Most prominently, La^{3+} addition yields little alteration in the kinetics of $Co(NH_3)_5F^{2+}$ electroreduction under these conditions, whereas the k_{app} values for $Co(NH_3)_5OSO_3^+$ as well as $Co(NH_3)_5Ac^{2+}$ (Ac = acetate) are diminished by ca 3-4 fold. Nevertheless, the 3-5 fold larger k_{app} values

observed on the I($\sqrt{7}$ x $\sqrt{7}$) relative to the I(3 x 3) adlayers are largely retained in the La^{3+} - containing electrolyte (Table I). This strongly suggests that the rate differences observed between these two adlayer structures are not due primarily to diffuse-layer effects (vide infra).

The electroreduction kinetics of the aromatic carboxylate-containing complexes differ distinctly in that the k_{app} values are not only similar on the two Pt/I adlayer surfaces, but are virtually unaffected by the addition of La^{3+}. For the cyclopentane-containing substituent, instead, significant (ca 2 fold) rate *increases* are obtained upon La^{3+} addition (Table I). These results attest to a likely specific role of the organic substituents upon the electrode kinetics.

A possible complication in the present measurements is that a lower-coverage (0.33) iodine adlattice, having ($\sqrt{3}$ x $\sqrt{3}$)R30° symmetry, is observed to form at relatively negative potentials on Pt(111) on the basis of in-situ STM images[4b] and also from LEED measurements.[2c] This potential-induced structural transformation is irreversible in the absence of solution iodide. The formation of the lower-coverage iodine structure during the voltammetric kinetic measurements, however, was deemed to be unlikely from the uniform observation of the appropriate ($\sqrt{7}$ x $\sqrt{7}$) and (3 X 3) adlattice structures by STM after as well as before the electrochemical measurement.

It is instructive to examine the reactant-dependent rate parameters on the iodine-adlayers in conjunction with corresponding data obtained on unmodified metal surfaces. To this end, Table I also contains k_{app} and α_{app} values obtained on unmodified Pt(111) and mercury electrodes in acidified 0.1 M $NaClO_4$. The latter surface is of particular interest here in view of the detailed double-layer analyses that have been undertaken for these and related reactions at the mercury-aqueous interface.[3b,6-8] Comparison between these kinetic data reveals several points of significance. Most noticeably,

substantial (up to ca 10^3 fold) differences in k_{app} are observed for a given reactant between the various electrode surfaces, the reactivity order being typically Hg < Pt/I(3 x 3) < Pt/I($\sqrt{7}$) < Pt. In view of the occurrence of significant perchlorate specific adsorption on mercury, the diffuse-layer corrected rate constants on this metal are typically 5-10 fold smaller than k_{app}.[3b,6,7] Even accounting for the qualitatively similar diffuse-layer effects observed on the Pt/I surfaces as for mercury (vide supra), the markedly (ca 10-100 fold) larger k_{app} values obtained at the former interfaces seem unlikely to be due primarily to this factor. This contention is supported by the uniformly more facile k_{app} values obtained on the Pt/I versus the Hg surface, irrespective of the net reactant charge Z (Table I), e.g. for X = NH_3, F^-, and OSO_3^{2-} (where Z_r = 3, 2, and 1, respectively).

Another instructive observation is that the systems yielding the largest k_{app} values tend also to exhibit large α_{app} values, ca 0.8-1.0. Such large α_{app} values obtained on the Pt/I surfaces are nevertheless virtually unaffected by the marked alterations in the diffuse-layer structure caused by the addition of La^{3+} (Table I), suggesting the occurrence of reaction sites inside the outer Helmholtz plane (oHp).[9, 18] (This is because the potential at such reaction sites close to the metal surface can constitute a large fraction of the overall interfacial potential, yielding substantial increases in the cationic reactant concentration at the reaction site as the electrode potential becomes more negative, and hence resulting in larger α_{app} values).

The observation of such large α_{app} as well as k_{app} values for the Pt/I surfaces in comparison with mercury is perhaps surprising since the presence of such densely packed iodine adlayers might be expected to oblige outer-sphere pathways to necessarily be followed, thereby involving reaction sites separated significantly from the metal surface. (Note that the van der Waals and covalent diameter of iodine atoms are 0.43 and 0.26 nm[19]). Especially

given the likelihood that the reaction sites at mercury lie inside the oHp[6,18], therefore, the facile electron-transfer kinetics observed at the iodine adlayer structures are noteworthy.

Even more facile electron-transfer rates are obtained for some of the present systems on unmodified Pt(111), the k_{app} values for X = NH_3, F^-, and OH_2 on this surface being 10-100 fold larger than on the iodine-coated surfaces. Extremely rapid kinetics have also been reported for these reactions on monocrystalline gold surfaces.[9] At least for the Pt(111)-aqueous interface, however, uncertainties in the extent of perchlorate anion adsorption complicate the data interpretation. It is worth noting that the differences in k_{app} between the unmodified and iodine-coated Pt(111) surfaces are minimized for $Co(NH_3)_5OSO_3^+$, as expected if these rate variations are due primarily to more favorable diffuse-layer effects at the former interface.

Kinetic Interpretation: Comparisons with STM Properties of Iodine Adlayers

In order to interpret further such environmental influences upon redox reactivity, it is convenient to express k_{app} as[1]

$$k_{app} = K_p \nu_n \kappa_{el} \exp(-\Delta G^*/RT) \qquad (2)$$

where K_p is the equilibrium constant (cm) for forming the interfacial precursor state geometrically favorable for electron transfer from the bulk-phase reactant, ν_n is the nuclear frequency factor, and ΔG^* is the free-energy barrier for the elementary electron-transfer step. Besides alterations in the electronic transmission coefficient κ_{el}, substrate-induced variations in k_{app} can arise from alterations in K_p and/or in ΔG^*.[1] Differences in diffuse-layer or other electrostatic double-layer effects, alluded to above, influence k_{app} predominantly via variations in K_p. Alterations in the spatial reaction site are also expected to exert important influences upon ΔG^* associated with the solvating environment and from surface imaging

effects.[20,21]

The larger electron-transfer rates observed on the Pt/I surfaces compared with mercury may well be due to enhancements in both κ_{el} and K_p, and possibly to diminutions in ΔG^*. The last factor is difficult to estimate. One can envisage direct contact between the reactant, probably involving the Co(III) pentaammine moiety, and the iodine adlayer; the resulting partial desolvation should diminish somewhat the solvent reorganization component of ΔG^*. The likely electrostatic attraction between the cationic reactants and the electronegative iodine adlayer, noted above, will act to increase k_{app} by enhancing K_p.

Alterations in κ_{el} brought about by variations in the substrate electronic properties refer directly to the electron-tunneling properties of the interface. Given that STM images provide a spatially resolved representation of electron-tunneling efficiencies between the substrate and the probe tip, the notion presents itself that the outer-sphere electron mediating properties of the ordered iodine adlayers may be related to the intensity of the corresponding STM images. There is no clearcut evidence that the observed rate differences between the ($\sqrt{7}$ x $\sqrt{7}$) and (3 x 3) adlayer structures are due predominantly to differences in κ_{el} rather than in K_p and/or ΔG^*. Nonetheless, careful examination of the STM results in relation to the kinetic data is instructive in this regard.

Inspection of crystallographic data[22] shows that the effective radius of the Co(III) pentaammine moiety, ca 0.35 nm, is not greatly different from the size of an iodine adatom. Moreover, one can envisage a reaction site where three facial ammine ligands are placed in a "tripod" arrangement onto a single adsorbed iodine, thereby bringing the Co(III) redox center close to the metal surface. This notion of a reaction site involving a single iodine adatom provides a simple basis with which to explore likely reasons

for the noticeably more efficient electron mediation to Co(III) provided by the ($\sqrt{7}$ x $\sqrt{7}$) as compared with the (3 x 3) iodine adlayers.

Recalling the STM structural information summarized above, a unique feature of the ($\sqrt{7}$ x $\sqrt{7}$) adlattice is the presence of iodine in hcp threefold hollow sites; one third of the iodines occupy these sites, along with equal occupancies in atop and fcc hollow sites (Fig. 2A). The significant feature of the hcp site in the present context is that it provides STM tunneling currents that are comparable to those for the atop site at least for smaller iodine-tip distances d (i.e. once account is taken of the different z positions of the threefold hollow and atop sites, vide supra). Given that the molecular reactant will presumably be able to approach equally closely to the iodines in threefold hollow and atop sites, it is reasonable to assert that the hcp site could provide a germane reaction center.

Although this reasoning is somewhat speculative, an additional argument supporting the electron-mediating ability of the hcp site is that placing a facial trio of ammine ligands onto the hcp iodine can bring the nitrogens into close proximity with the three underlying platinum atoms. Especially given that the electron is transferred into a σ orbital on Co(III),[23] having lobes lying along the cobalt-nitrogen bond axis, such a reactant geometry might be expected to engender an especially large donor-acceptor orbital overlap, and hence yield a larger κ_{el} provided that the reaction pathway remains nonadiabatic. The importance of the underlying Pt atomic arrangement to the electron-tunneling efficiency is highlighted by the strikingly smaller STM currents observed at the fcc versus the hcp sites (Figs. 1,3). As mentioned above, the latter geometry features an additional second-layer Pt atom immediately underneath the iodine adatom (Fig. 2A).

Identification of such "preferred" reaction sites for electron transfer on the ($\sqrt{7}$ x $\sqrt{7}$) versus the (3 x 3) adlayers is complicated by the simul-

taneous presence of a pair of (3 x 3) adlayer structures, so that it is unfortunately not possible to discern the relative contributions of the "hex" and "asym" adlattices to the measured reaction rates on the (3 x 3) adlayer. Nevertheless, the occurrence of 1/3 and 2/3 atop iodines in the hex and asym structures (Figs. 2B,C), together with the observed comparable populations of these adlattices in the (3 x 3) adlayer, leads to the conclusion that this site is more prevalent than in the ($\sqrt{7}$ x $\sqrt{7}$) adlattice, which features only 1/3 atop sites (Fig. 2A). From this it can be deduced that the atop iodines do not provide an especially facile reaction site, although the clustered trios of asymmetric-atop iodines in the (3 x 3)-asym adlattice may offer a rather different reaction environment than the more "isolated" symmetric atop sites in (3 x 3)-hex and ($\sqrt{7}$ x $\sqrt{7}$).

Of course, we do not wish to imply that such atop iodine sites do not contribute significantly to the reaction rate. It is nonetheless noteworthy that these sites, which yield the most intense STM images, do not appear to provide the prevalent electron-transfer pathways for the present Co(III) ammine reactants: if that were the case, tne (3 x 3) adlayer would be expected to yield the more facile kinetics. As already noted, factors other than electron-tunneling efficiency may be partly responsible for the observed rate differences on the ($\sqrt{7}$ x $\sqrt{7}$) and (3 x 3) adlayers. Although the charge densities present on the various iodine adatoms are unknown, it is feasible that the hcp (and possibly the fcc) sites on the ($\sqrt{7}$ x $\sqrt{7}$) adlattice could provide an electrostatically favored reaction environment. The significantly larger k_{app} values observed for the present outer-sphere reactions on the ($\sqrt{7}$ x $\sqrt{7}$) relative to the (3 x 3) adlayer structures may therefore reflect enhanced values of both κ_{el} and K_p at the former interface.

Examination of the electroreduction rate parameters for the Co(III) ammines containing organic carboxylate substituents on the iodine adlayers

is also of interest, especially in view of the markedly (up to 10^3 fold) enhanced reactivities afforded by these moieties at unmodified mercury electrodes.[8,24] These rate enhancements are due apparently to incipient adsorption of the hydrophobic groups on the metal surface, thereby increasing k_{app} via larger values of K_p and possibly also κ_{el}. A suitable "reference" reaction with which to examine the carboxylate complex reactivities is $Co(NH_3)_5Ac^{2+}$ reduction, since this structurally similar acetate ligand lacks only the rate-enhancing cyclic organic substituents (see ref. 8 for details).

Scrutiny of the rate data in Table I shows that significantly (up to ca 10 fold) larger k_{app} values are obtained for the two carboxylate complexes containing aromatic substituents (benzene and pyridine), while little or no rate accelerations are afforded by the aliphatic cyclic substituent cyclopentane. Other differences between the aromatic- and aliphatic-containing reactants is that the former exhibit barely noticeable rate differences between the ($\sqrt{7}$ x $\sqrt{7}$) and (3 x 3) adlayer surfaces, which are largely unaffected by the addition of La^{3+} ions. This behavior indicates that the aromatic substituents induce significantly different, as well as more facile, electroreduction pathways at the Pt/I electrodes, probably via specific aromatic-iodine adsorbate interactions. Nevertheless, the rate enhancements induced by the aromatic substituents on the Pt/I surfaces are milder than observed at mercury (Table I).

Overall, then, the Pt(111) iodine-adlayers provide unusually well-defined electrode surfaces having in some respects known and adjustable electronic structural properties. The characterization of such surfaces by atomic-resolution STM can yield unique real-space electronic as well as structural information for this purpose. Admittedly, the connection between the molecular electron-transfer kinetics and the tunneling properties as revealed by STM for the present systems did not turn out to be as straightforward as we ex-

pected initially. Nonetheless, the examination of a wider range of one-electron outer-sphere reactions on these and other surfaces characterized in parallel by STM appears well worthwhile, offering the prospect of a deeper appreciation of the role of electronic factors in electrochemical kinetics.

Acknowledgments

This work is supported in part by grants from the National Science Foundation and the Office of Naval Research (to MJW) and the Industrial Associates Program at Purdue University funded in part by Dow Chemical Co. and BP America (to BCS).

References and Notes

1. For a review, see Weaver, M. J., in "Comprehensive Chemical Kinetics", Vol. 27, Compton, R. G., Elsevier, Amsterdam, 1987, Chapter 1.

2. (a) Lane, R. F.; Hubbard, A. T., J. Phys. Chem., **1975**, 79, 808; (b) Felter, T. E.; Hubbard, A. T., J. Electroanal. Chem., **1979**, 100, 473; (c) Hubbard, A.T., Chem. Rev., **1988**, 88, 633.

3. (a) Barr, S. W.; Weaver, M. J., Inorg. Chem., **1984**, 23, 1657; (b) Guyer, K. L.; Barr, S. W.; Cave, R. J.; Weaver, M. J., "Proc. 3rd Symposium on Electrode Processes", Bruckenstein, S.; McIntyre, J. D. E.; Miller, B.; Yeager, E., eds, Electrochemical Society, Pennington, NJ, 1980, p. 390.

4. (a) Schardt, B. C.; Yau, S-L; Rinaldi, F., Science, **1989**, 243, 1050; (b) Yau, S-L; Vitus, C. M.; Schardt, B. C., J. Am. Chem. Soc., **1990**, 112, 3677.

5. Zurawski, D.; Rice. L.; Hourani, M.; Wieckowski, A., J. Electroanal Chem., **1987**, 230, 221.

6. (a) Weaver, M. J.; Satterberg, T. L., J. Phys. Chem., **1978**, 82, 1784; (b) Weaver, M. J., J. Electroanal. Chem., **1978**, 93, 231.

7. Barr, S. W.; Guyer, K. L.; Weaver, M. J., J. Electroanal. Chem., **1980**, 111, 41.

8. (a) Li, T -T. T; Weaver, M. J., Inorg. Chem., **1985**, 24, 1882; (b) Tadayyoni, M. A.; Weaver, M. J., J. Electroanal. Chem., **1985**, 187, 283.

9. Hamelin, A.; Weaver, M. J., J. Electroanal. Chem., **1986**, 209, 109.

10. Leung, L-W. H.; Wieckowski. A.; Weaver, M. J., J. Phys. Chem., **1988**, 92, 6985.

11. Schardt, B.C., Rev. Sci. Inst., in press.

12. Katekaru, J. Y.; Garwood, Jr., G. A.; Herschberger, J.; Hubbard, A. T., Surface Sci., **1982**, 121, 396.

13. Similar relations have been discussed and employed for electron tunneling between pairs of metal surfaces as in STM[14a] and also for nonadiabatic electron transfer between molecular redox sites[14b] or between metal surfaces and molecular sites.[14c,d]

14. For example: (a) Hansma, P. K.; Tersoff, J., J. Appl. Phys., **1987**, 61,

R1; (b) Logan, J.; Newton, M. D., J. Chem. Phys., **1983**, 78, 4086; (c) Morgan, J. D.; Wolynes, P. G., J. Phys. Chem., **1987**, 91, 874; (d) Li, T.T-T.; Weaver, M. J., J. Am. Chem. Soc., **1984**, 106, 6106.

15. Soler, J.M.; Baró, A.M.; Garcia, N.; Rohrer, H., Phys. Rev. Lett., **1986**, 57, 444.

16. The chemical irreversibility of the Co(III) electroreductions thwarts determination of the Co(III)/(II) formal potentials. This is inconsequential, however, for the present purposes that involve rate comparisons between different interfaces for a given reaction at an electrode potential corresponding to a fixed, albeit unknown, overpotential.

17. Weaver, M. J.; Anson, F. C., J. Electroanal. Chem., **1975**, 65, 711, 737.

18. Also see: Weaver, M.J.; Liu, H.Y.; Kim, Y., Can J. Chem., **1981**, 59, 1944.

19. Gordon, A. J.; Ford, R. A., "The Chemists Companion", Wiley-Interscience, New York, 1972, pp. 82, 109.

20. Kharkats, Yu I.; Nielson, H.; Ulstrup, J., J. Electroanal. Chem., **1984**, 169, 47.

21. Phelps, D. K.; Kornyshev, A. A.; Weaver, M. J., J. Phys. Chem., **1990**, 94, 1454.

22. (a) Kime, N. E.; Ibers, J. A., Acta Cryst. B., **1969**, 25, 168; (b) Kruger, G. J.; Reynhardt, E. C., Acta Cryst. B, **1978**, 34, 915.

23. (a) Newton, M. D., J. Phys. Chem., **1986**, 90, 3734; (b) Newton, M. D., J. Phys. Chem., **1988**, 92, 3049.

24. The data columns in Table I of ref. 8a labelled "mercury electrode" and "gold electrode" are unfortunately interchanged due to a typesetting error. That is, the data given in this Table obtained at mercury are the right-hand pair of columns, not the left-hand columns.

TABLE I Rate Parameters for the Electroreduction of $Co^{III}(NH_3)_5X$ Complexes at -0.1 V vs SCE on Pt(111)/I, Pt(111), Hg Surfaces at 23°C.

$Co^{III}(NH_3)_5X$ reactant	Surface[a]	Electrolyte[b]	k_{app}[c,d] cm s^{-1}	α_{app}[d,e]
$X = NH_3$	Pt/I($\sqrt{7}$)	0.1 M $NaClO_4$	3×10^{-3}	1.05
		+50 mM La^{3+}	2×10^{-4}	1.0
	Pt/I(3x3)	0.1 M $NaClO_4$	8×10^{-4}	1.05
		+50 mM La^{3+}	1.0×10^{-4}	1.0
	Pt	0.1 M $NaClO_4$	$\approx 1 \times 10^{-2}$	0.95
	Hg	0.1 M $NaClO_4$	1.7×10^{-5}	0.7
F^-	Pt/I($\sqrt{7}$)	0.1 M $NaClO_4$	7×10^{-4}	0.75
		+50 mM La^{3+}	7×10^{-4}	0.75
	Pt/I(3x3)	0.1 M $NaClO_4$	2×10^{-4}	0.75
		+50 mM La^{3+}	2×10^{-4}	0.75
	Pt	0.1 M $NaClO_4$	4×10^{-2}	0.85
	Hg	0.1 M $NaClO_4$	2×10^{-5}	0.6
OSO_3^{2-}	Pt/I($\sqrt{7}$)	0.1 M $NaClO_4$	3.5×10^{-2}	0.65
		+50 mM La^{3+}	9×10^{-3}	0.65
	Pt/I(3x3)	0.1 M $NaClO_4$	8×10^{-3}	0.65
		+50 mM La^{3+}	2×10^{-3}	0.7
	Pt	0.1 M $NaClO_4$	1.8×10^{-2}	0.74
	Hg	0.1 M $NaClO_4$	6×10^{-5}	≈ 0.5
OH_2	Pt/I$\sqrt{7}$	0.1 M $NaClO_4$	~0.15	0.85
		+50 mM La^{3+}	2×10^{-2}	0.8
	Pt/I(3x3)	0.1 M $NaClO_4$	3×10^{-2}	0.75
		+50 mM La^{3+}	8×10^{-3}	0.65
	Hg	0.1 M $NaClO_4$	1.0×10^{-3}	0.5
CH_3COO^-	Pt/I$\sqrt{7}$	0.1 M $NaClO_4$	1.5×10^{-3}	0.85
		+50 mM La^{3+}	3×10^{-4}	0.9
	Pt/I(3x3)	0.1 M $NaClO_4$	4×10^{-4}	0.85
		+50 mM La^{3+}	1.0×10^{-4}	0.85
	Pt	0.1 M $NaClO_4$	4.5×10^{-2}	0.75
	Hg	0.1 M $NaClO_4$	3×10^{-5}	0.7

[continued on next page]

TABLE I (continued)

$Co^{III}(NH_3)_5X$ reactant	Surface[a]	Electrolyte[b]	k_{app}[c,d] $cm\ s^{-1}$	α_{app}[d,e]
$C_6H_5CH_2COO^-$	Pt/I(√7)	0.1 M $NaClO_4$	4×10^{-3}	0.7
		+50 mM La^{3+}	4×10^{-3}	0.7
	Pt/I(3x3)	0.1 M $NaClO_4$	4×10^{-3}	0.7
		+50 mM La^{3+}	3.5×10^{-3}	0.7
	Pt	0.1 M $NaClO_4$	5.5×10^{-4}	0.7
	Hg	0.1 M $NaClO_4$	6.5×10^{-3}	0.65
$p\text{-}C_5H_4NCOO^-$	Pt/I√7	0.1 M $NaClO_4$	3×10^{-3}	0.9
		+50 mM La^{3+}	4.5×10^{-3}	0.75
	Pt/I(3x3)	0.1 M $NaClO_4$	1.5×10^{-3}	0.8
		+50 mM La^{3+}	1.5×10^{-3}	0.75
	Hg	0.1 M $NaClO_4$	1.3×10^{-3}	0.85
$C_5H_9CH_2COO^-$	Pt/I√7	0.1 M $NaClO_4$	2.5×10^{-4}	0.95
		+50 mM La^{3+}	5.5×10^{-4}	0.75
	Pt/I(3x3)	0.1 M $NaClO_4$	7×10^{-5}	0.8
		+50 mM La^{3+}	$\sim 1 \times 10^{-4}$	
	Hg	0.1 M $NaClO_4$	5×10^{-4}	0.75

FOOTNOTES TO TABLE I

[a] Key to abbreviations: Pt/I√7 = Pt(111) surface with (√7 x √7) iodine adlayer; Pt/I(3 x 3) = Pt(111) with (3 x 3) iodine adlayer, as deduced from STM (see text for details); Pt = Pt(111) annealed surface, after iodine removal (see text). Hg = dropping mercury electrode.

[b] All electrolytes contained ca 5 mM $HClO_4$; La^{3+} added as $La(ClO_4)_3$.

[c] Observed rate constant for electrooxidation at -0.1 V vs SCE.

[d] Values for Pt surfaces determined in the present work by using linear sweep voltammetry in outlined in the text and ref. 9; values for Hg taken mostly from refs. 7 and 8.

[e] Observed transfer coefficient for electroreduction within potential range ca 0 to -0.2 V vs SCE.

FIGURE CAPTIONS

Fig. 1

($\sqrt{7}$ x $\sqrt{7}$)R19.1° adlattice of iodine on Pt(111). The rhombic cell is outlined in black. Representative iodine adsorption sites are labeled. Tunneling conditions: bias voltage V_b = 0.9 mV, i_o = 20.0 nA.

Fig. 2

Schematics of the three iodine adlattice structures: (a) ($\sqrt{7}$ x $\sqrt{7}$)R19.1°; (b) (3 x 3)-hex; (c) (3 x 3)-asym.

Fig. 3

z-x cross sections through STM images of the ($\sqrt{7}$ x $\sqrt{7}$)R19.1° adlattice of iodine. The cross sections were taken through the long axis of the unit cell, see Figure 1. The images were acquired under the following conditions: 1MΩ, V_b = 20 mV, i_t = 20 nA; 250 KΩ, V_b = 5 mV, i_t = 20 nA; 100 KΩ, V_b = 2 mV, i_t = 20 nA; 50 KΩ, V_b = 1 mV, i_t = 20 nA.

Fig. 4

STM image of (3 x 3)-hex iodine adlattice on Pt(111). The rhombic unit cell is outlined in black. Representative iodine adsorption sites are labeled. Tunneling conditions: V_b = 0.9 mV, i_o = 20.0 nA.

Fig. 5

STM image of (3 x 3)-asym iodine adlattice on Pt(111). The rhombic unit cell is outlined in black. Representative iodine adsorption sites are labeled. Tunneling conditions: V_b = 0.9 mV, i_o = 20.0 nA.

Fig. 6

(a) z-x cross sections through STM images of the (3 x 3)-hex adlattice of iodine. The cross sections were taken through the long axis of the unit cell, see Figure 4. The images were acquired under the following conditions: 1MΩ, V_b = 20 mV, i_t = 20 nA; 500 KΩ, V_b = 10 mV, i_t = 20 nA; 60 KΩ, V_b = 0.9 mV, i_t = 15 nA. (b) z-x cross through an STM image of the (3 x 3)-asym adlattice of iodine. The cross section was taken through the a-axis of the unit cell as to pass through iodine atoms at asym and fcc sites, see Figure 4. The STM image was acquired with V_b = 2.1 mV, i_t = 10 nA.

Fig. 7

(a) STM image of a domain boundary between (3 x 3)-hex and (3 x 3)-asym iodine adlattices, V_b = 4.0 mV, i_o = 15 nA. The arrow superimposed on the image indicates the direction of the z-x cross section shown in Figure 7b; (b) z-x cross section through STM image shown in Figure 7a.

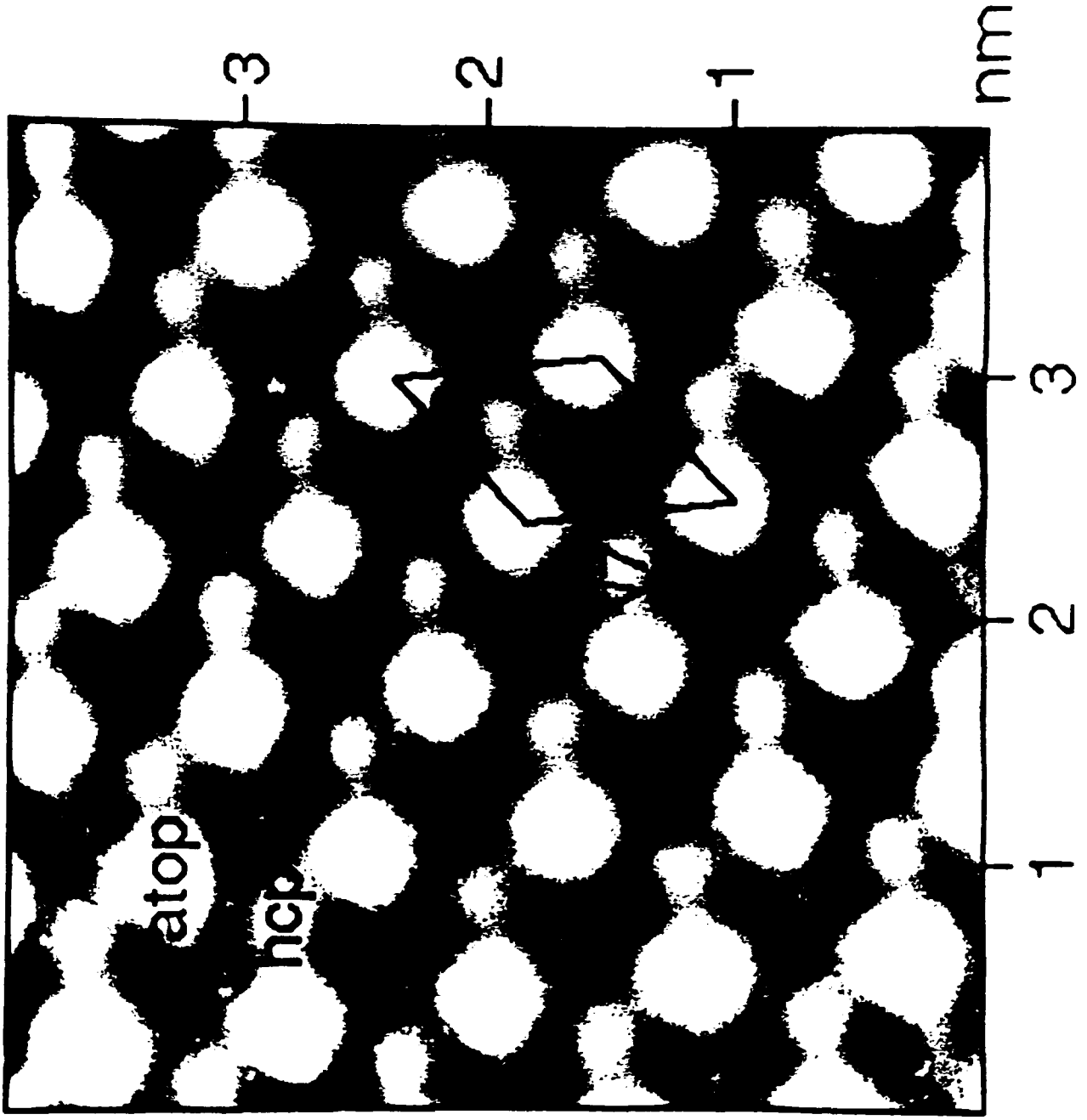

CHANG ET AL

FIG 1

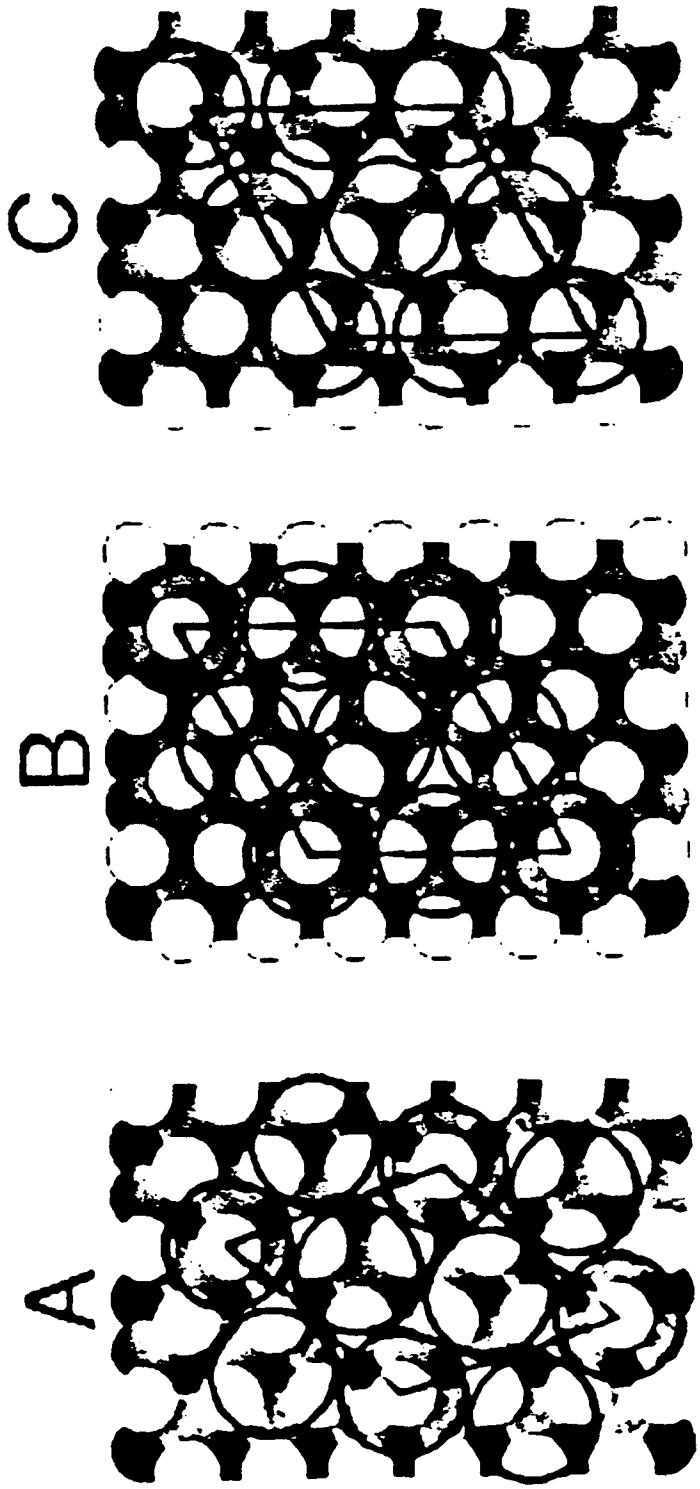

CHANG ET AL

FIG 2

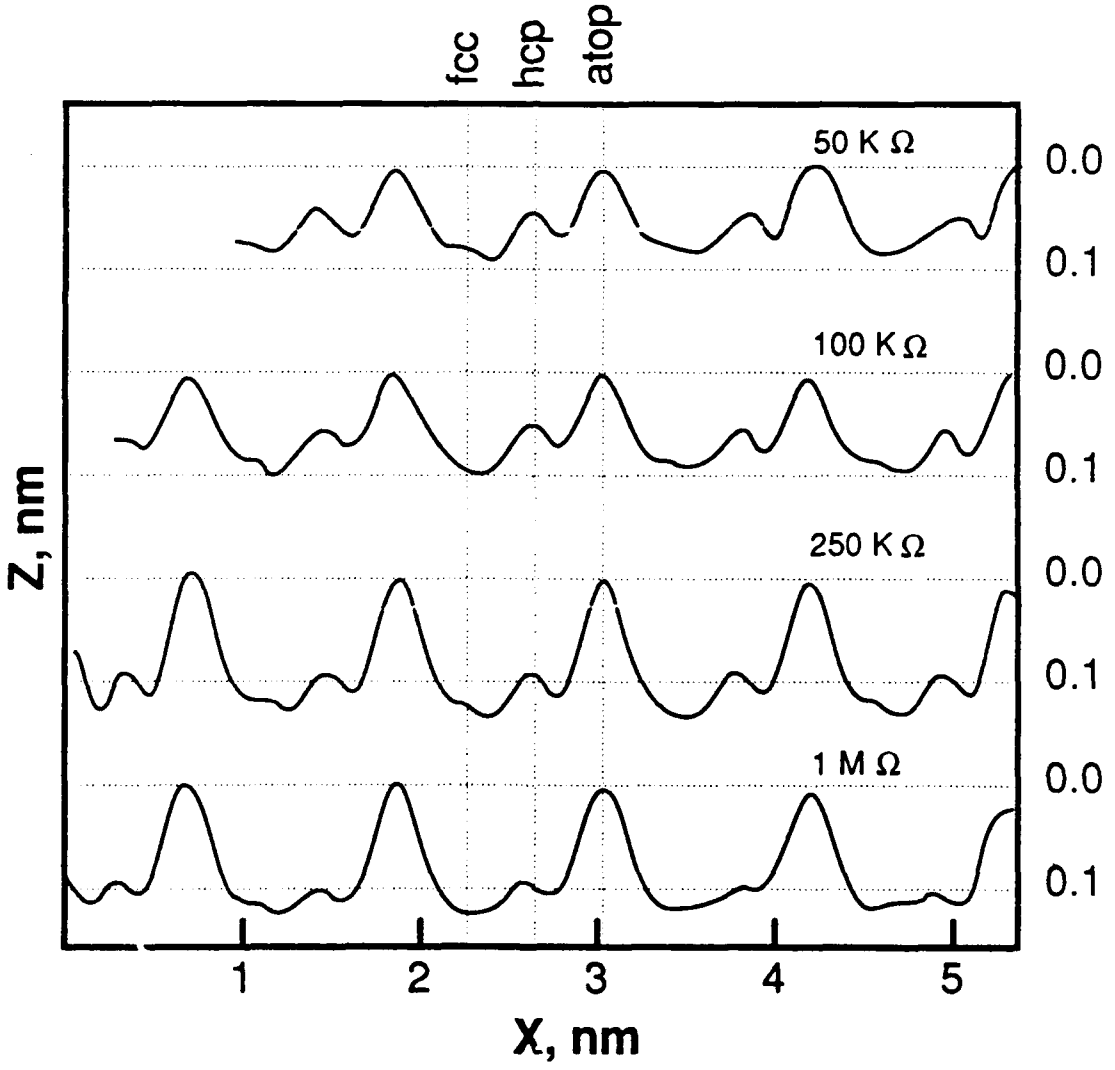

CHANG ET AL

FIG 3

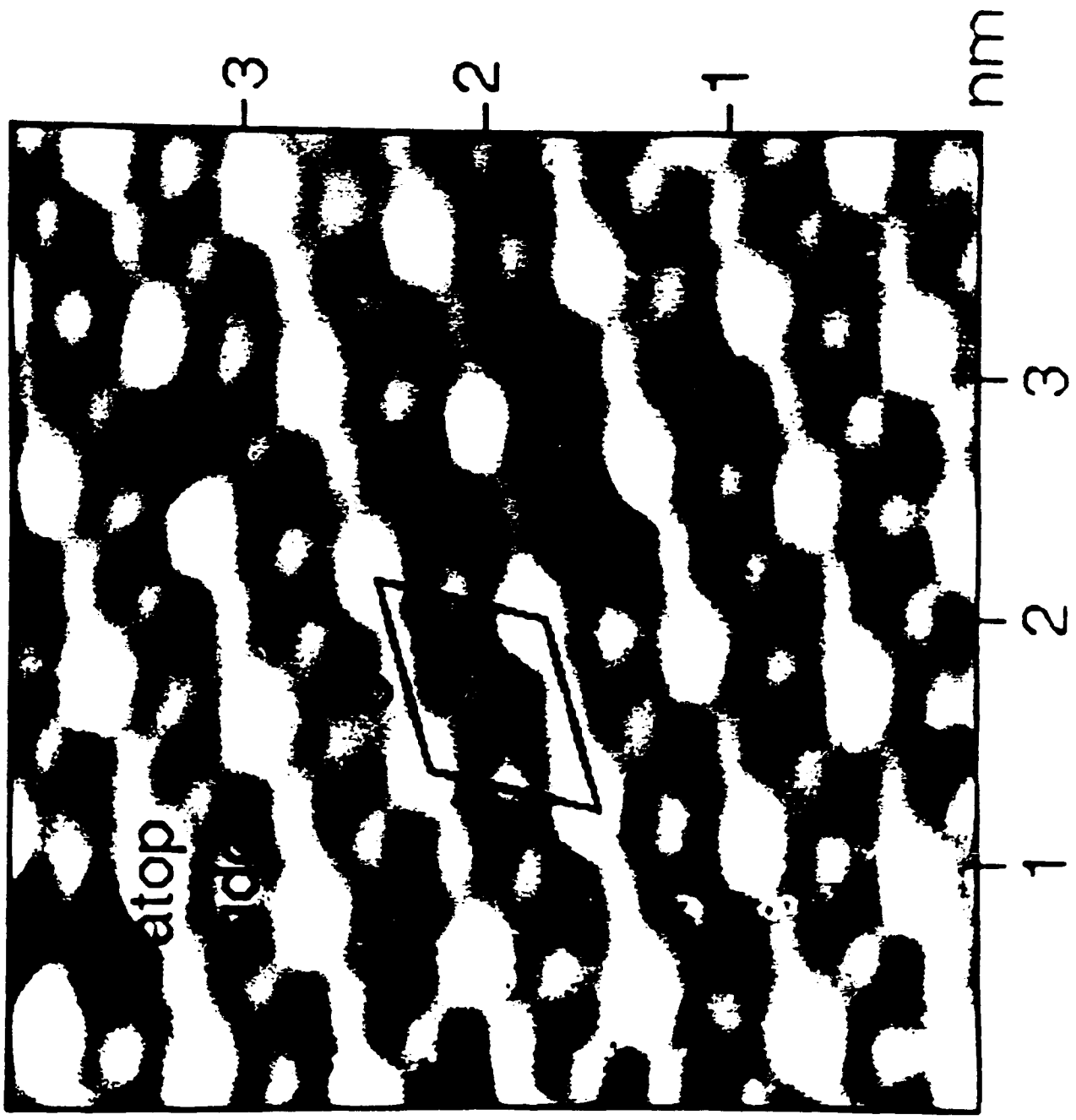

CHANG ET AL

FIG 4

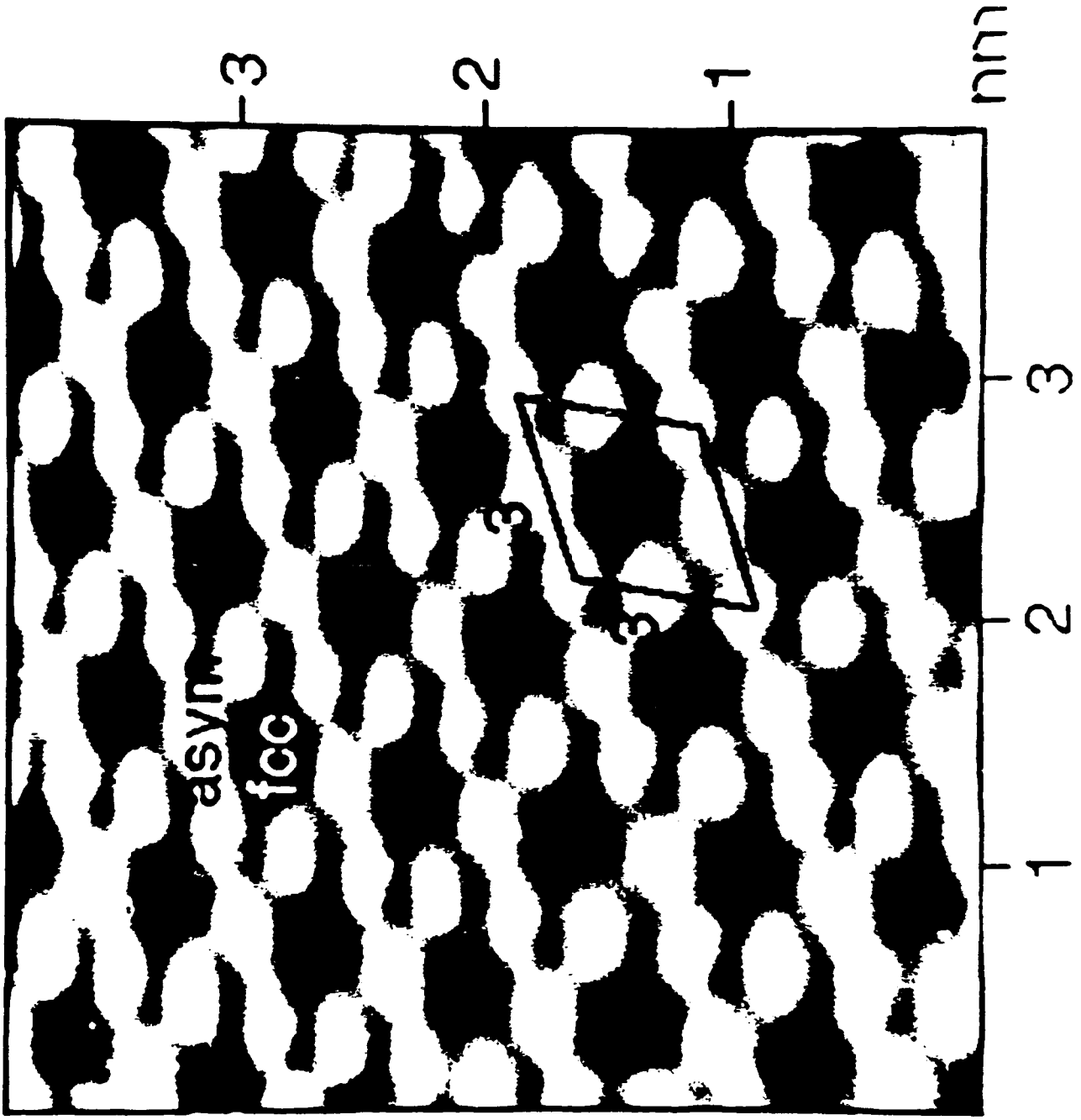

CHANG ET AL

FIG 5

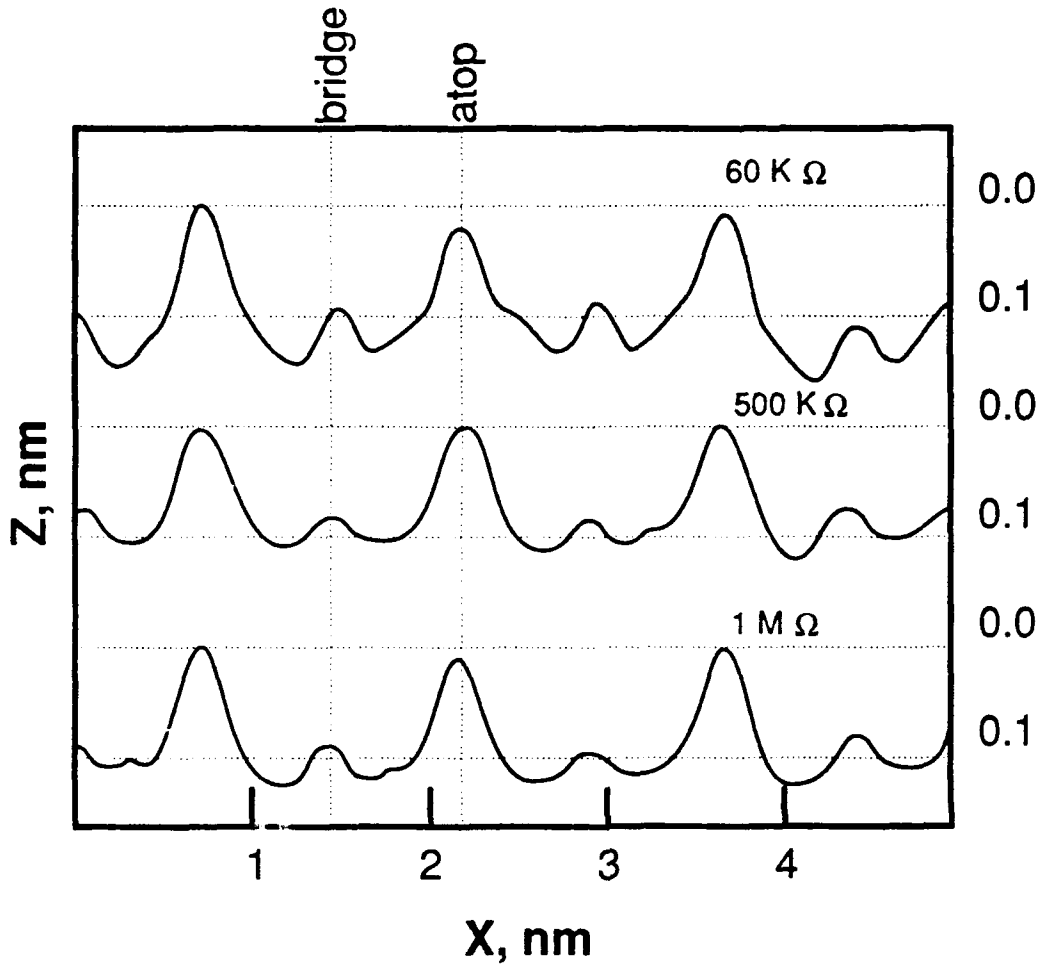

CHANG ET AL
FIG 6A

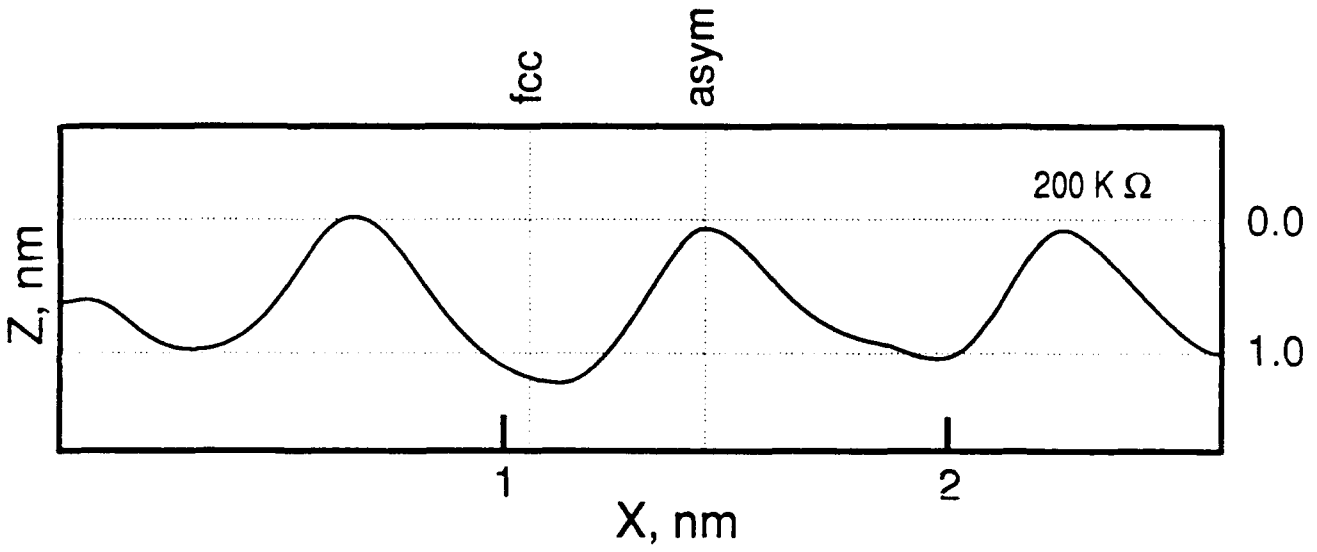

CHANG ET AL
FIG 6B

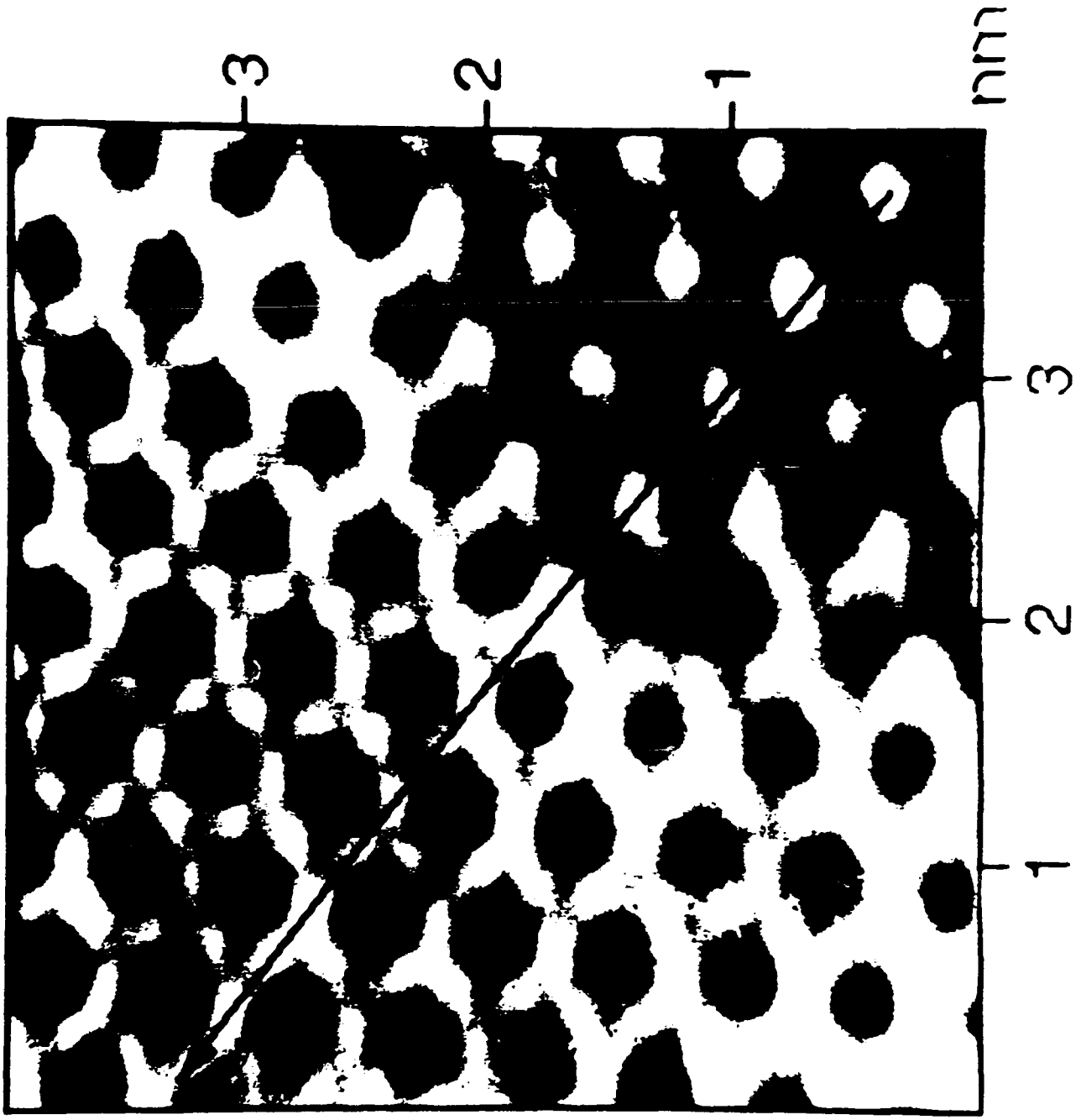

CHANG ET AL

FIG 7A

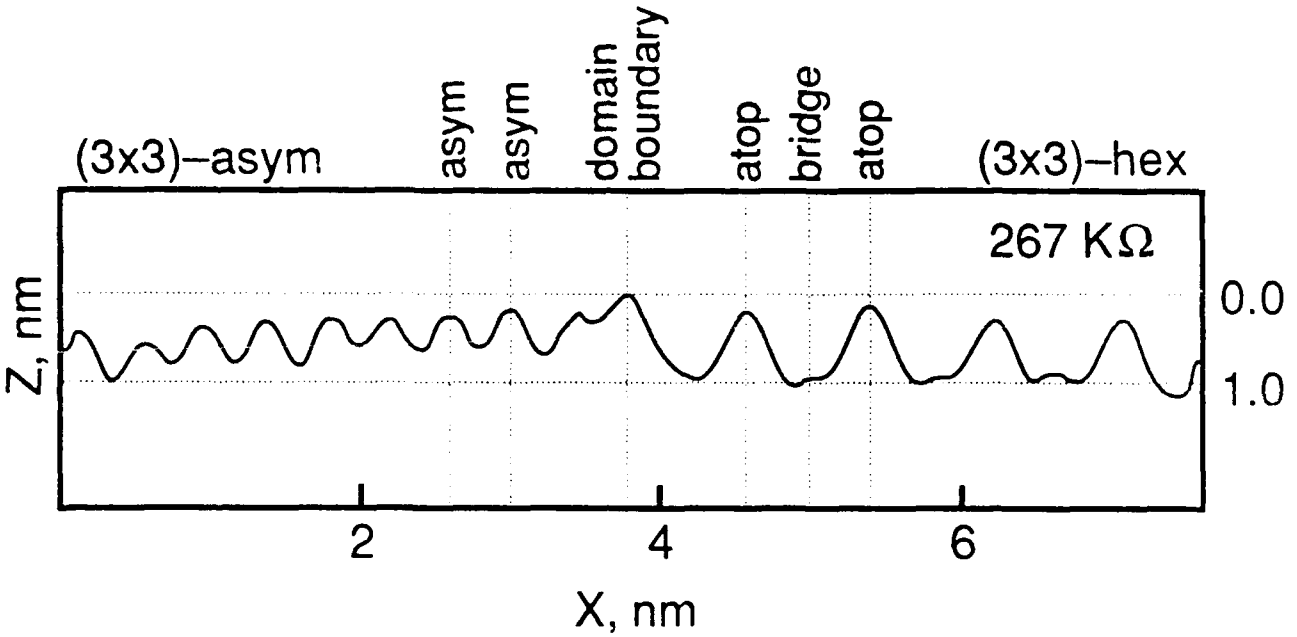

CHANG ET AL
FIG 7B